All-Optical Modulation in a Silicon Waveguide Based on a Single-Photon Process

Tom Baehr-Jones, Michael Hochberg, and Axel Scherer

(Invited Paper)

***Abstract*—All-optical, low-power modulation is a major goal in photonics. Because of their high mode-field concentration and ease of manufacturing, nanoscale silicon waveguides offer an intriguing platform for photonics. So far, all-optical modulators built with silicon photonic circuits have relied on either two-photon absorption or the Kerr effect. Both effects are weak in silicon, and require extremely high (∼5 W) peak optical power levels to achieve modulation. Here, we describe an all-optical Mach–Zehnder modulator based on a single-photon absorption (SPA) process, fabricated entirely in silicon. Our SPA modulator is based on a process by which a single photon at 1.55 μm is absorbed and an apparently free-carrier-mediated process causes an index shift in silicon, even though the photon energy does not exceed that of silicon's bandgap. We demonstrate all-optical modulation with a gate response of 1°/mW at 0.5 Gb/s. This is over an order of magnitude more responsive than typical previously demonstrated devices. Even without resonant enhancement, further engineering may enable all optical modulation with less than 10 mW of gate power required for complete extinction, and speeds of 5 Gb/s or higher.**

***Index Terms*—Integrated optics, nonlinear optics, optical modulation.**

I. Introduction

BECAUSE silicon has a bandgap of 1.12 eV, it is an ideal material platform for near-infrared integrated optical circuits [1], [2]. Electrically driven modulation [3] and an optically pumped silicon laser have been previously demonstrated [4]. For all-optical signal processing applications, low-power all-optical modulation is critical [5], [6]. Applications would include optical buffering [7], all-optical wavelength conversion [8], and all-optical computation [9], [10]. Almeida *et al*. and Foerst *et al*. have recently demonstrated an all-optical modulator with single-photon absorption (SPA) based carrier injection using visible light [11], [12]. This approach has severe limitations; because of the disparate wavelengths for gate and signal, these devices cannot be cascaded into circuits that require feedback.

Recently, Geis *et al*. demonstrated an efficient photodetector at 1.55 μm based on an SPA mechanism [13], achieving greater than 50% quantum efficiency at speeds up to 10 GHz. It utilized absorption centers created in a waveguide by ion damage, which enabled the absorption of photons at energies below the bandgap. SPA was also observed in undamaged samples, and attributed to surface-state absorption. Similar linear photocurrent responses have been observed elsewhere, both due to volume defects and solely due to the waveguide surface states [14]–[16]. It has been hypothesized that defects create mid-bandgap states, enabling an electron to reach the conduction band from the valence band, but the precise mechanism is not yet fully understood [13].

It is well known that surface states cause optical loss in silicon waveguides [17]. Most low-loss geometries involve large silicon waveguides, on scales of 0.450 μm × 0.250 μm [18] and 2 μm × 0.9 μm [19], which minimize the interaction of the optical mode with surface states. In our SPA modulator, we use a smaller 0.5 × 0.1 μm ridge waveguide [20], resulting in a very large electric field at the etched surfaces. By electrically contacting the silicon waveguides, we have demonstrated that a linear photocurrent can be observed, with a quantum efficiency of 2.8% [16]. In our other work, the region responsible for the photocurrent was identified as the waveguide surface, though the precise mechanism was not determined.

II. Device Layout and Test

A. Layout

Here, we use the surface-absorption process to build an all-optical modulator: we introduce a gate optical mode into one arm of a Mach–Zehnder interferometer. The SPA process occurs, and an unbalanced refractive index shift occurs in one of the arms, causing constructive or destructive interference in a signal beam. Fig. 1 shows a diagram of the device geometry. The arm lengths of the devices that we tested ranged from 0.75 to 1.25 cm, and the arms were unequal in length within each device, with differences ranging from 150 to 600 μm. This inequality allows us to control the intrinsic phase shift between the arms by tuning the signal wavelength. Typical waveguide losses in these devices were 6 dB/cm. Input coupling is achieved from a polarization-maintaining fiber array via grating couplers [20].

The device performance is best characterized by the phase shift induced per unit gate power. A gate response of 1°/mW corresponds to around 180 mW for complete extinction of the signal mode, if the gate response remains linear at higher powers. This power level, which we call P_π, is analogous to the V_π associated with an electrooptic modulator [21].

Manuscript received January 8, 2008. Current version published October 3, 2008. This work was supported in part by the National Science Foundation in part by the Defense Advanced Research Projects Agency (DARPA) under the Electronic and Photonic Integrated Circuits (EPIC) Program HR-04-1-0054, and in part by the Air Force Office of Scientific Research Young Investigator Program under Grant FA9550-08-0101.

T. Baehr-Jones and M. Hochberg are with the University of Washington, Seattle, WA 98195 USA (e-mail: baehrjt@washington.edu; hochberg@washington.edu).

A. Scherer is with the California Institute of Technology, Pasadena, CA 91125 USA (e-mail: etcher@caltech.edu).

Digital Object Identifier 10.1109/JSTQE.2008.920292

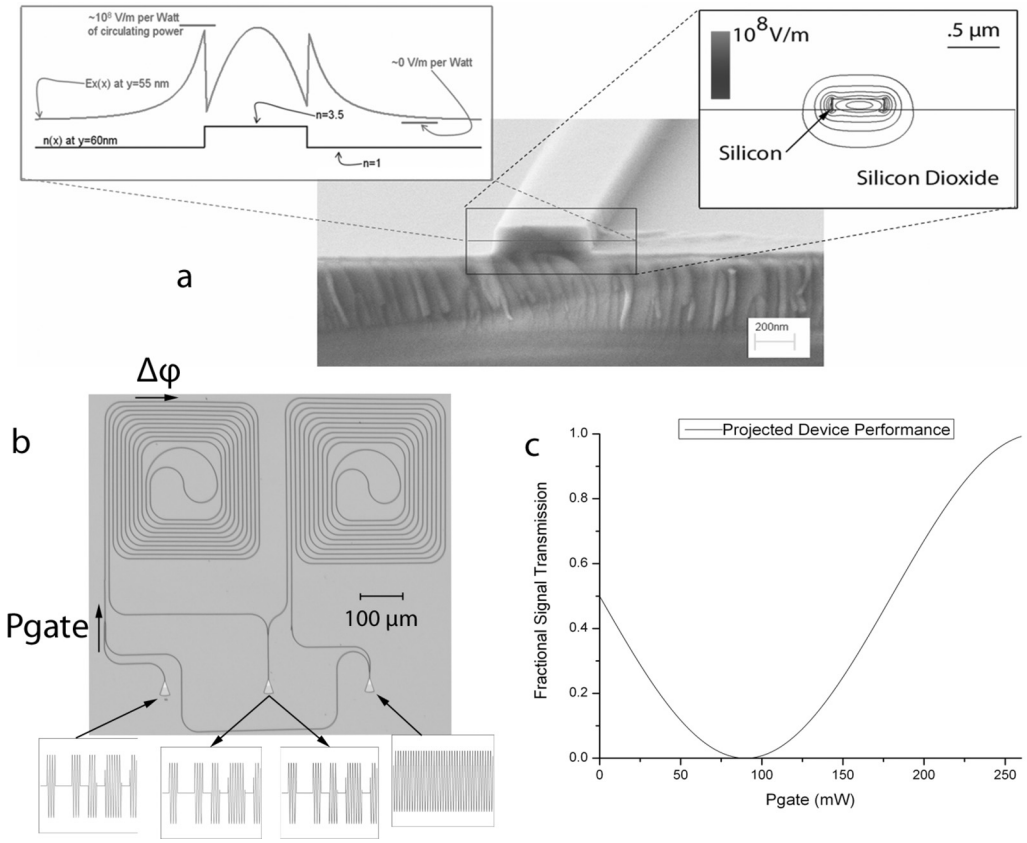

Fig. 1. Diagram of waveguide and device layout. (a) SEM micrograph of cleaved ridge waveguide with modal patterns illustrated. (b) Optical image of the SPA modulator, with the gate and signal optical modes illustrated. P_{gate} indicates the location that the gate optical mode is mixed into a Mach–Zehnder arm with a y-junction, and begins to cause a phase delay, labeled $\Delta\varphi$, in the signal mode. The gate power as reported in the paper is always the propagating power at this point in the waveguide. Thought not visible in this image, there is a corresponding y-junction on the opposing arm, ensuring that the Mach–Zehnder is balanced. (c) Idealized transmission of the signal is shown for a device with a gate response of 1°/mW, and a bias point of 90°.

B. Fabrication Information

Devices were fabricated in electronics-grade silicon-on-insulator (SOI) supplied by Soitec, doped at around 10^{15} dopants (boron)/cm^3. No implant or irradiation was performed on the silicon material. The starting material was thinned to about 110 nm by dry oxidation, separated into small chips, and patterned with electron beam lithography using a 100 kV electron beam writer using hydrogen silsesquioxane (HSQ) resist. The samples were etched with chlorine in an inductively coupled plasma etcher. No cladding layer was deposited.

C. Testing With Pseudorandom Bit Sequence

Initial testing was done by modulating the gate beam with a pseudorandom bit sequence. A modulated gate optical mode on the order of 25 mW propagating power in the waveguide with 50% extinction was used, and this was directed into the gate port of the modulator. To assist the measurements and enhance the effect by increasing the optical power levels, two erbium-doped fiber amplifiers (EDFAs) were used. The signal beam was set to a wavelength such that there was an intrinsic 90° modulator bias point. We obtained eye diagrams at 300 and 500 Mb/s, as shown in Fig. 2.

It is important to note in Fig. 2 that the spectral filter placed in the modulator output preferentially removes the original gate optical frequency, leaving only the signal frequency. As a result, the open eye pattern demonstrates that the bit pattern on the gate mode has been transferred via the all-optical modulator to the signal mode. This type of operation is likely to be of use in the construction of future all-optical networks [8].

D. Characterization With Sinusoidal Excitation

To better understand the device response with lower gate powers, and to characterize the frequency dependence of the mechanism, testing was performed with a gate having a sinusoidal intensity modulation. A lock-in amplifier was also used. Fig. 3 shows typical results; here an SPA modulator achieved a response to the gate of 0.6°/mW. We used a frequency of 32 MHz, a gate wavelength of 1541 nm, and a signal wavelength of 1550.8 nm to test SPA modulators with varying arm lengths, frequencies, and wavelengths. The extinction on the sinusoidal modulation was around 20%.

We measured the dependence of the device response on the signal wavelength. As shown in Fig. 3, the maximum response occurred at bias points of 90 or -90°; this is the location of the maximum response for a phase-modulation-based effect. This is compelling evidence that the SPA mechanism primarily causes phase modulation, not intensity modulation. Changing the gate wavelength did not lead to a notable change in device

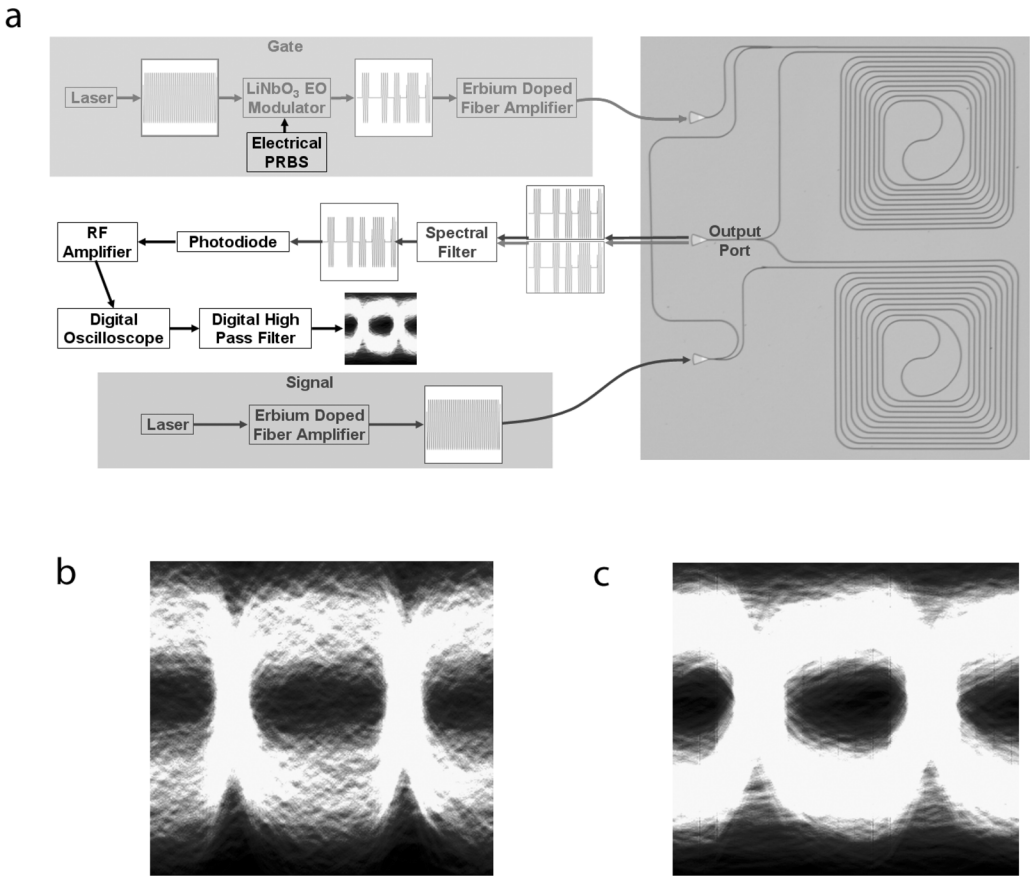

Fig. 2. Description of eye-pattern experiment. (a) Diagram of the experimental setup used to measure the response of the SPA modulator and obtain an eye-pattern. (b) Eye pattern obtained at 300 Mb/s. (c) Eye pattern obtained at 500 Mb/s.

performance; this is as expected, since at no point does the gate mode interfere with itself, nor should the phase of the gate mode affect the signal mode.

The data shown in Fig. 3 also provide insight into the quantum mechanism behind the all-optical modulation. In particular, a single-photon mechanism is suggested. If the modulation were based on a two-photon process, then the increase in peak-to-peak output intensity should be quadratic in increasing gate powers. Note that, as in the pseudorandom bit sequence experiments, a filter has been used to selectively view only the signal optical mode.

E. Frequency Dependence

The frequency of the sinusoidal gate modulation was varied, and further data were taken to determine the bandwidth of the all-optical modulation mechanism. As before, a lock-in amplifier was used along with a filter to isolate the signal optical mode on the device output. As detailed in Fig. 4, data were taken at speeds from 30 kHz to 50 MHz. The device response was fairly flat from 1 to 50 MHz; the higher response at slower speeds is likely due to heating.

Higher speed data were taken by means of a lightwave component analyzer (LCA). In this case, an Agilent 8703B was used. As before, a spectral filter was used to remove the gate mode from the output of the device, ensuring that the LCA measured only the intensity modulation due to the all-optical modulation effect. Fig. 5 shows the results that were obtained. There is clearly a substantial falloff in the device response as the modulation speed approaches 1 GHz. As will be discussed shortly, this is evidence of free-carrier mediation.

F. Testing With a Pulse Stream

To measure the polarity of the mechanism, as well as to observe the performance at slightly higher levels of gate power, measurements were performed in which the gate was pulsed at a repetition rate of 30 MHz and a pulsewidth of 8 ns. The wavelength was chosen to utilize the arm length difference to bias the Mach–Zehnder offset θ, as it appears in (1) in Section III. It was found that the polarity of the phase shift was negative, that is, $\partial_\varphi / \partial P_{\mathrm{gate}}$ is negative. Device response of approximately -0.9°/mW was observed at a peak gate power of 33.5 mW for a total phase shift of -30°. A negative index shift is consistent with the effects free carriers, but not the Kerr effect or heating. Details are shown in Fig. 6.

III. Analysis

A. Evidence of Single-Photon Mechanism

There are a number of possible mechanisms by which one near-infrared optical mode can induce a phase shift in a second

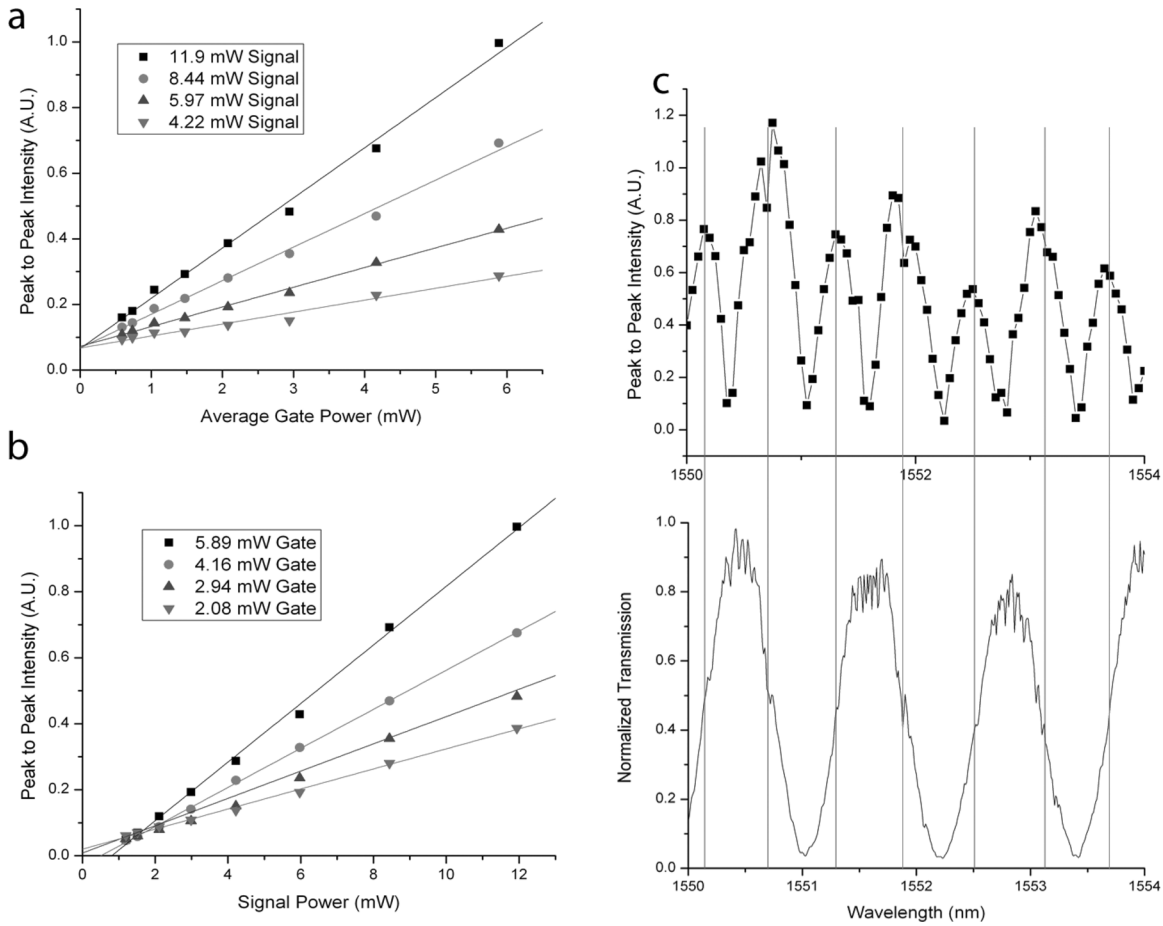

Fig. 3. Results of lock-in-amplifier-assisted measurements. (a) Device response, in peak-to-peak intensity of modulated signal, as a function of gate power. The extinction on the gate is about 20%. The signal power reported is the projected average power in the silicon waveguide just before the initial Mach–Zehnder *y*-junction. (b) Device response in similar circumstances as a function of varying signal power. In both cases, a linear relation is observed. (c) Device response as a function of signal wavelength, as well as the passive transmission through the SPA modulator of the signal alone. Maximum response is found at 90° and 270° bias points, which have 50% signal mode transmission, corresponding to a phase modulation mechanism.

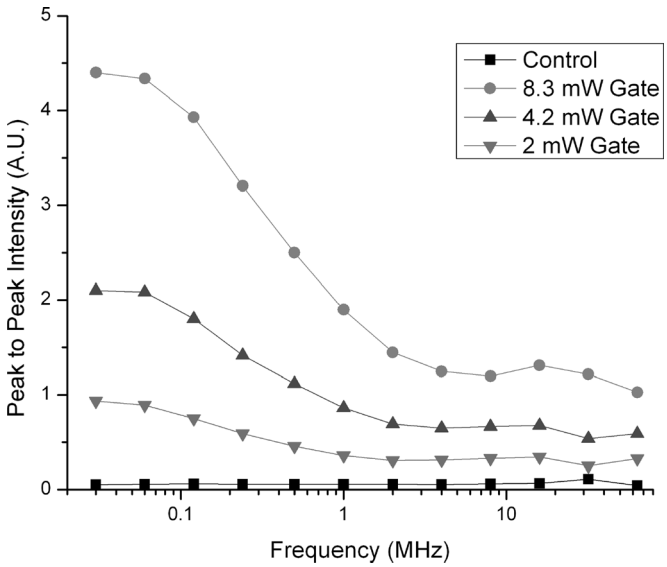

Fig. 4. Frequency-dependent device response at slower speeds. The peak-to-peak intensity modulation measured on the output gate mode is shown as a function of gate modulation frequency for a constant gate power. The larger response close to 1 MHz is likely due to thermal effects becoming important.

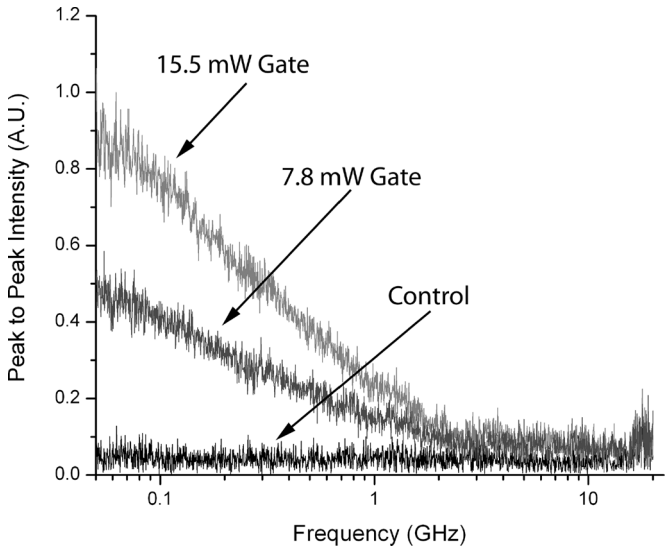

Fig. 5. High-speed frequency response of device. As before, the peak-to-peak intensity modulation measured on the output gate mode is shown as a function of gate modulation frequency for a constant gate power. A control is shown in which the signal power was set to zero and the gate to around 15.5 mW, confirming that the gate mode has been filtered out fully.

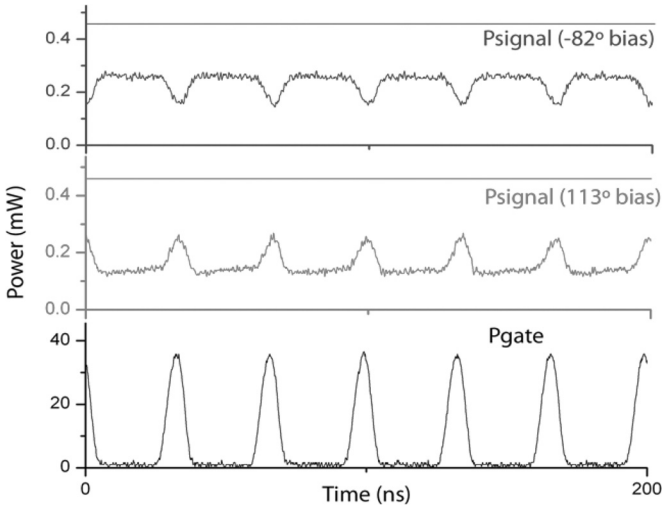

Fig. 6. Results of pulsed measurements. The projected time-domain trace of the gate power is shown in one curve. The data have been normalized so that the known insertion loss due to the grating couplers has been removed; as a result, the power shown is the propagating power in the modulation waveguide. The output signal powers are shown for two different bias points; in this case, the power reported is the projected power in the silicon waveguide past the final Mach–Zehnder *y*-junction.

near-infrared optical mode in a silicon waveguide. These consist of thermal interaction [24], the Kerr effect [22], or free-carrier dispersion, which can be due to two-photon absorption (TPA) [9], or in the case of our all-optical modulator SPA. Whatever the mechanism, it is possible to express the all-optical interaction as

$$P_{\text{out}} = C\left(1+\cos\left(\gamma\left(\left(1+b\cos\left(\omega t\right)\right)P_{\text{gate}}\right)^{\alpha}+\theta\right)\right)P_{\text{signal}}^{\beta} \tag{1}$$

where we have assumed that the gate signal has the form

$$\left(1+b\cos\left(\omega t\right)\right)P_{\text{gate}}. \tag{2}$$

Here, P_{out} is the output power as a function of time of the filtered signal optical mode, and γ and C are proportionality constants characteristic of the interaction. We have also assumed that the signal is at a speed far below the bandwidth limit of the relevant effect. If the modulator is biased at the point of maximal response, that is, choosing θ to be $\pm\pi/2$, then the peak-to-peak intensity modulation on the output will be proportional to

$$R \propto 2\gamma b^{\alpha} P_{\text{gate}}^{\alpha} P_{\text{signal}}^{\beta} \tag{3}$$

if the modulation effect produces much less than $\pi/2$ radians of phase shift. In all of the experiments described in Section II, except where explicitly noted otherwise, the modulator bias was always set to this value. It was easy to do this, because far less than $\pi/2$ radians of shift was achieved in even the highest gate power cases, and so this amounted to simply tuning the signal wavelength to maximize the device response. In the case of a linear modulation mechanism, that is, where α and β are both 1, γ can be identified as $\partial_{\varphi}/\partial P_{\text{gate}}$.

Other than SPA, the mechanisms that exhibit this power law are TPA-based absorption modulation [10], the Kerr effect [22], and Raman scattering [4]. In all three cases, however, there exists no bandwidth limitation near 1 GHz. Of these effects, a phase shift would be observed for only the Kerr effect. Moreover, Raman scattering must involve wavelengths separated by the Raman shift—15.6 THz in silicon [4]—which is clearly irrelevant to the current result. As shown in Table I, the observed gate response is also more than an order of magnitude larger than what would be achievable with any mechanism other than SPA, even in an idealized case. SPA is the only mechanism consistent with the observed data.

The lower gate responses of other modulation mechanisms result in typical effective P_{π} values from 5 W [4], [9] to 100 W [22]. The high modulation power requires most other devices to be operated in pulsed mode. Even when resonant enhancement is used to greatly lower the external power required, the internal circulating power must still be quite high [9], [25], [26]. By contrast, our SPA-based device can be projected to achieve complete extinction at around 180 mW P_{π}, over an order of magnitude lower than that achieved with existing mechanisms. No further resonant enhancement would be required. Furthermore, silicon nanowaveguides can carry bit streams with average power levels in the tens and hundreds of milliwatts; multiwatt average power levels will rapidly damage the guides [27].

B. Free-Carrier Model of Modulation Effect

If the hypothetical model of the creation of both an electron and hole is used, the shift in electron–hole concentration can be written as

$$\Delta N = \tau\frac{\sigma}{A}P. \tag{4}$$

Here, P is the gate power, A is the waveguide area, and we introduce σ, the absorption density, which determines the number of photons absorbed per unit length in the waveguide for a given amount of power. The absorption density has units of inverse of centimeters per second per watt. The parasitic loss from absorption will be

$$\alpha = h\nu\sigma. \tag{5}$$

Here, h is Planck's constant and ν is the relevant photon frequency, around 193 THz.

We could then express the device response using the following free-carrier dispersion relations [3]:

$$\frac{\partial\phi}{\partial P_{\text{gate}}} = -\frac{\partial}{\partial P_{\text{gate}}}\int_0^L dz\left(\left(P_{\text{gate}}\exp\left(-\alpha z\right)\frac{\tau\sigma}{A}+p_0\right)^{0.8}8.5\times10^{-18}+\left(P_{\text{gate}}\exp\left(-\alpha z\right)\frac{\tau\sigma}{A}+n_0\right)8.8\times10^{-22}\right)\frac{\partial n_{\text{eff}}}{\partial n_{\text{bulk}}}\times k_0. \tag{6}$$

A similar expression would be used if only a free hole were created, and would in fact provide comparable results, since free holes have a larger influence on the induced refractive index shift. Here, A is the waveguide area, p_0 and n_0 are equilibrium hole and electron concentrations, P_{gate} is the gate power, τ the recombination lifetime, σ is the absorption density, and α is the

TABLE I
ALL-OPTICAL MODULATION MECHANISMS IN SILICON WAVEGUIDES

Effect	α	β	Bandwidth	Theoretical maximum gate response near 5 mW (degrees/mW)	Typical effective gate response near 5 mW (degrees/mW)
Electro-optic modulation	N/A	1	Free carrier limited	N/A	N/A
Carrier injection from TPA (I)	2	1	Free carrier limited	0.1	7×10^{-5} [9]
Carrier injection from TPA (II)	1	2	Free carrier limited	N/A	N/A
TPA based absorption	1	1	Ultrafast	N/A	N/A
Kerr Effect	1	1	Ultrafast	0.14	0.0018 [22]
Stimulated Raman scattering	1	1	Raman gain bandwidth, 100 GHz	N/A	N/A
Single-photon absorption (This work)	1	1	Apparently free carrier limited	32	1

List of all-optical modulation mechanisms in silicon waveguides. For each mechanism, the two exponents from (3) are shown. For phase modulation mechanisms, the theoretical gate response for the silicon ridge waveguide studies is given for powers near 5 mW. Also shown is the response achieved in an actual realization. The device response for SPA, representing the devices reported in this letter, is for a 1.2 cm Mach-Zehnder modulator, with gate power near 5 mW. We have assumed that the shift in refractive index is linearly proportional to the number of free carriers, which is approximately valid in the relevant optical power regime, in writing the exponents [2]. We have also assumed that the bandwidth of the SPA mechanism is limited by the free-carrier lifetime [23]. The discrepancy between the theoretical and observed performance is due in part to the larger waveguides used in typical realizations, compared to the 0.5 x 0.1 μm ridge assumed here, as well as effective lengths that may be less that 1.2 cm. Since carrier injection from TPA (II) is not linear in the input signal, it is impossible to quantify a comparable gate response. The estimate of the SPA modulator's theoretically best performance assumes that an electron and hole are created with each absorbed photon. One of the works referred to utilizes resonant enhancement is [9]; for clarity of comparison, the projected performance in a nonresonant Mach-Zehnder modulator is shown. Note that the achieved performance in our device exceeds the theoretical limit for the Kerr effect as well as carrier-injected TPA (I).

optical attenuation coefficient. Equation (6) will be nearly linear in the regime for which data were taken.

Equation (6) implicitly assumes that the operation speed is much lower than the bandwidth limitation. As is shown in the Appendix, as the operation speed approaches the recombination lifetime, the device response in the form of peak-to-peak intensity of the modulated signal:

$$R \propto \frac{1}{\sqrt{1+(\omega\tau)^2}}. \tag{7}$$

Here, ω is the excitation frequency and τ is the minority-carrier lifetime. As a result of (1), the device response will have a 70% reduction at around $f = 1/2\tau$. This occurs near 1 GHz, suggesting a minority carrier lifetime of around 0.5 ns, similar to values reported elsewhere for similar SOI ridge waveguides [9]. This provides further evidence that the modulation effect is free-carrier mediated.

C. Calculating Surface-State Absorption Density

Equation (6) can be solved for the observed phase shift once the recombination lifetime is known. In the case of the highest performing device, which achieved around 16.6° for 15.5 mW of gate power, the absorption density can be calculated as $1.4 \times 10^{14}(\text{cm}\cdot\text{s}\cdot\text{mW})^{-1}$. This implies a waveguide loss due to the SPA mechanism of only 0.1 dB/cm, a small fraction of the waveguide loss seen. Typical excess carrier concentrations under testing conditions with this density are on the order of 7×10^{14} cm^{-3} for 5 mW of gate power.

In the case of Geis *et al*. [13], the absorption density is measured directly through a photocurrent measurement. A responsivity of 0.8 A/W was demonstrated in a 0.25 mm device, corresponding to a quantum efficiency of 64%. This implies that the optical loss due solely to absorption would be at least 178 dB/cm, and from (3), the absorption density can be estimated as $3.1 \times 10^{17}(\text{cm}\cdot\text{s}\cdot\text{mW})^{-1}$.

D. Ultimate Performance Limitations

Further work will be required to understand the SPA mechanism. One possibility is that an electron is excited into the conduction band from the valence band. Or perhaps the electron is knocked into a defect state, creating a free hole. As holes have a disproportionately large effect on the refractive index shift in silicon [2], the creation of a free hole would adequately explain the observed behavior.

If we hypothesize that both an electron and a hole are created for each absorbed photon, we can estimate the ultimate performance limits. The free-carrier lifetime would determine the ultimate modulation speed [23]. Approaches have been developed to lower this lifetime and frequencies exceeding 5 Gb/s should be possible [28]. It is also possible to decrease the gate power required for modulation by increasing the density of photon-absorption centers, at the expense of insertion loss. We estimate that allowing 6 dB of additional loss from implantation-generated defect centers, a gate response of 32°/mW could be achieved at 0.5 Gb/s, corresponding to a P_π of around 6 mW; this would require around a factor of 100 increase in absorption density over the value currently obtained in our devices.

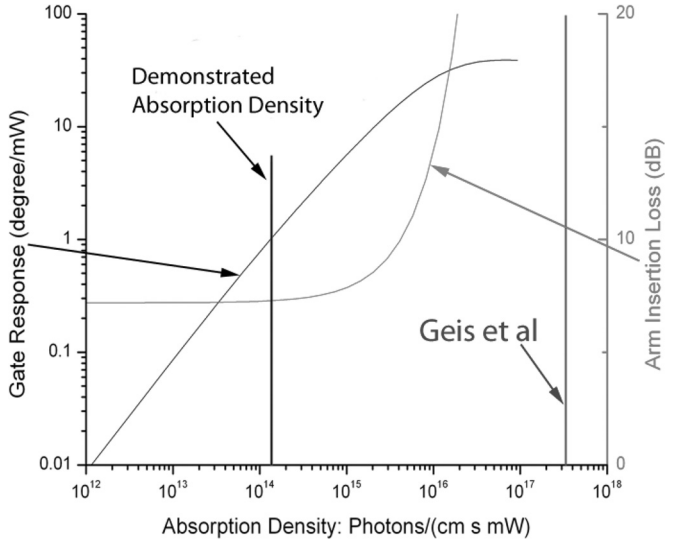

Fig. 7. Projected performance of device for varying surface-state absorption densities. A response of nearly 32°/mW could be obtained for absorption densities a factor of 100 higher than the projected value in our device.

Absorption center densities as much as three orders of magnitude higher than those in this paper have been previously engineered [13], suggesting that these improvements are likely to be possible. Fig. 7 shows a chart of projected performance values for varying absorption densities.

IV. Conclusion

We have demonstrated all-optical modulation in silicon with a novel single-photon mechanism. Our device achieves modulation at power levels an order of magnitude lower than typical all-optical modulators in silicon. We believe that bandwidths in the tens of gigahertz and peak modulation powers on the scale of 10 mW are achievable. With such performance, it will be possible to obtain broadband all-optical signal gain, enabling chip-scale optical transistors to be integrated into all-optical integrated logic circuits.

Appendix

Derivation of Bandwidth Limit for Device

The response of the Mach–Zehnder near the 3 dB bias point of the modulator is proportional to the phase shift induced by the gate signal. This in turn is nearly proportional to the free-carrier density. As a result, the frequency response can be calculated based on the time-dependent equation for the excess carrier concentration [29]:

$$\frac{dN}{dt} = G - \frac{N}{\tau}. \tag{8}$$

Here, G is the generation rate in inverse centimeters cube per second. Under the experimental conditions of a gate with a sinusoidal intensity modulation, $G(t)$ will have the form $G_0(1 + b\cos(\omega t))$. The solution for N in this case is

$$N(t) = G_0\tau\left(1 + \mathrm{Re}\left(\frac{\exp(i\omega t)}{1 + i\omega\tau}\right)\right). \tag{9}$$

Since the responsivity is proportional to the ac amplitude of $N(t)$, it will have a frequency dependence of $(1 + (\omega t)^2)^{-1/2}$.

Acknowledgment

The authors acknowledge J. Huang, B. Penkov, and A. Homyk for assistance with the measurements and imaging. They also acknowledge Prof. S. Dunham for a number of useful discussions. Device fabrication was performed at the Cornell Nanoscale Facility.

References

[1] M. Lipson, "Guiding, modulating and emitting light on silicon—Challenges and opportunities," *J. Lightw. Technol.*, vol. 23, no. 12, pp. 4222–4238, Dec. 2005.
[2] R. A. Soref and B. R. Bennett, "Electrooptical effects in silicon," *IEEE J. Quantum Electron.*, vol. QE-23, no. 1, pp. 123–129, Jan. 1987.
[3] A. Liu, R. Jones, L. Liao, D. Samara-Rubio, D. Rubin, O. Cohen, R. Nicolaescu, and M. Paniccia, "A high-speed silicon optical modulator based on a metal–oxide–semiconductor capacitor," *Nature*, vol. 427, pp. 615–618, 2004.
[4] H. S. Rong, Y. H. Kuo, S. B. Xu, A. S. Liu, R. Jones, and M. Paniccia, "Monolithic integrated Raman silicon laser," *Opt. Exp.*, vol. 14, pp. 6705–6712, 2006.
[5] M. Hochberg, T. Baehr-Jones, G. X. Wang, M. Shearn, K. Harvard, J. D. Luo, B. Q. Chen, Z. W. Shi, R. Lawson, P. Sullivan, A. K. Y. Jen, L. Dalton, and A. Scherer, "Terahertz all-optical modulation in a silicon–polymer hybrid system," *Nat. Mater.*, vol. 5, pp. 703–709, 2006.
[6] I. Fushman, E. Waks, D. Englund, N. Stoltz, P. Petroff, and J. Vuckovic, "Ultrafast nonlinear optical tuning of photonic crystal cavities," *Appl. Phys. Lett.*, vol. 90, pp. 091118-1–091118-9, 2007.
[7] F. N. Xia, L. Sekaric, and Y. Vlasov, "Ultracompact optical buffers on a silicon chip," *Nat. Photon.*, vol. 1, pp. 65–71, 2007.
[8] Y. H. Kuo, H. S. Rong, V. Sih, S. B. Xu, M. Paniccia, and O. Cohen, "Demonstration of wavelength conversion at 40 Gb/s data rate in silicon waveguides," *Opt. Exp.*, vol. 14, pp. 11721–11726, 2006.
[9] Q. Xu and M. Lipson, "All-optical logic based on silicon micro-ring resonators," *Opt. Exp.*, vol. 15, pp. 924–929, 2007.
[10] T. K. Liang, L. R. Nunes, M. Tsuchiya, K. S. Abedin, T. Miyazaki, D. Van Thourhout, W. Bogaerts, P. Dumon, R. Baets, and H. K. Tsang, "High speed logic gate using two-photon absorption in silicon waveguides," *Opt. Commun.*, vol. 265, pp. 171–174, 2006.
[11] V. R. Almeida, C. A. Barrios, R. R. Panepucci, and M. Lipson, "All-optical control of light on a silicon chip," *Nature*, vol. 431, pp. 1081–1084, 2004.
[12] M. Först, J. Niehusmann, T. Ploetzing, J. Bolten, T. Wahlbrink, C. Moormann, and H. Kurz, "High-speed all-optical switching in ion-implanted silicon-on-insulator microring resonators," *Opt. Lett.*, vol. 32, pp. 2046–2048, 2007.
[13] M. W. Geis, S. J. Spector, M. E. Grein, R. T. Schulein, J. U. Yoon, D. M. Lennon, S. Deneault, F. Gan, F. X. Kaertner, and T. M. Lyszczarz, "CMOS-compatible all-Si high-speed waveguide photodiodes with high responsivity in near-infrared communication band," *IEEE Photon. Technol. Lett.*, vol. 19, no. 3, pp. 152–154, Feb. 2007.
[14] J. D. B. Bradley, P. E. Jessop, and A. P. Knights, "Silicon waveguide-integrated optical power monitor with enhanced sensitivity at 1550 nm," *Appl. Phys. Lett.*, vol. 86, pp. 241103-1–241103-3, 2005.
[15] Y. Liu, C. W. Chow, W. Y. Cheung, and H. K. Tsang, "In-line channel power monitor based on helium ion implantation in silicon-on-insulator waveguides," *IEEE Photon. Technol. Lett.*, vol. 18, no. 17, pp. 1882–1884, Sep. 2006.
[16] T. Baehr-Jones, M. Hochberg, and A. Scherer, "Photodetection in silicon beyond the band edge with surface states," *Opt. Exp.*, vol. 16, pp. 1659–1668, 2008.
[17] M. Borselli, T. J. Johnson, and O. Painter, "Measuring the role of surface chemistry in silicon microphotonics," *Appl. Phys. Lett.*, vol. 88, pp. 131114-1–131114-3, 2006.
[18] V. Almeida, R. Panepucci, and M. Lipson, "Nanotaper for compact mode conversion," *Opt. Lett.*, vol. 28, pp. 1302–1304, 2003.
[19] S. Fathpour, K. K. Tsia, and B. Jalali, "Energy harvesting in silicon Raman amplifiers," *Appl. Phys. Lett.*, vol. 89, pp. 061109-1–061109-3, 2006.
[20] T. Baehr-Jones, M. Hochberg, C. Walker, and A. Scherer, "High-Q ring resonators in thin silicon-on-insulator," *Appl. Phys. Lett.*, vol. 85, pp. 081101-1–081101-3, 2005.

[21] M. Hochberg, T. Baehr-Jones, G. Wang, J. Huang, P. Sullivan, L. Dalton, and A. Scherer, "Towards a millivolt optical modulator with nano-slot waveguides," *Opt. Exp.*, vol. 15, pp. 8401–8410, 2007.
[22] Ö. Boyraz, P. Koonath, V. Raghunathan, and B. Jalali, "All optical switching and continuum generation in silicon waveguides," *Opt. Exp.*, vol. 12, pp. 4094–4102, 2004.
[23] A. S. Liu, H. S. Rong, R. Jones, O. Cohen, D. Hak, and M. Paniccia, "Optical amplification and lasing by stimulated Raman scattering in silicon waveguides," *J. Lightw. Technol.*, vol. 24, no. 3, pp. 1440–1455, Mar. 2006.
[24] T. Baehr-Jones, M. Hochberg, C. Walker, E. Chan, D. Koshinz, W. Krug, and A. Scherer, "Analysis of the tuning sensitivity of silicon-on-insulator optical ring resonators," *J. Lightw. Technol.*, vol. 23, no. 12, pp. 4215–4221, Dec. 2005.
[25] A. Yariv, "Universal relations for coupling of optical power between microresonators and dielectric waveguides," *Electron. Lett.*, vol. 36, pp. 321–322, 2000.
[26] T. Tanabe, M. Notomi, S. Mitsugi, A. Shinya, and E. Kuramochi, "Fast bistable all-optical switch and memory on a silicon photonic crystal on-chip," *Opt. Lett.*, vol. 30, pp. 2575–2577, 2005.
[27] T. Baehr-Jones, M. Hochberg, R. Soref, and A. Scherer, "Design of a tunable, room temperature, continuous-wave terahertz source and detector using silicon waveguides," *J. Opt. Soc. Amer. B*, vol. 25, pp. 261–268, 2008.
[28] S. F. Preble, Q. Xu, B. Schmidt, and M. Lipson, "Ultra-fast all-optical modulation on a silicon chip," *Opt. Lett.*, vol. 30, pp. 2891–2893, 2005.
[29] S. M. Sze, *Physics of Semiconductor Devices*, 2nd ed. New York: Wiley, 1981.

Tom Baehr-Jones received the B.S. degree in physics and the M.S. and Ph.D. degrees in applied physics from California Institute of Technology (Caltech), Pasadena, in 2002, 2005, and 2006, respectively.

He is currently a staff member of the nanophotonics group at the University of Washington, Seattle. His current research interests include computational physics and the design and fabrication of nonlinear integrated optics devices. He is a cofounder of Luxtera, a silicon photonics company.

Michael Hochberg received the B.S. degree in physics and the M.S. and Ph.D. degrees in applied physics from California Institute of Technology (Caltech), Pasadena, in 2002, 2005, and 2006, respectively.

He cofounded Luxtera, a venture-funded company, where he spent a year full-time. He has worked on developing ultrafast nonlinear optical devices using silicon photonics, which included the development of all-optical switches operating at terahertz bandwidth, the integrated optical rectification based detectors, and a variety of other linear and nonlinear optical devices. He is currently a faculty member in electrical engineering at the University of Washington, Seattle.

Dr. Hochberg is the recipient of a National Science Foundation (NSF) Graduate Research Fellowship and a Caltech Upper Class Merit Award. He was also awarded the Demetriades-Tsafka Prize in Nanotechnology for the best thesis by a graduating Ph.D. student in the field of nanotechnology.

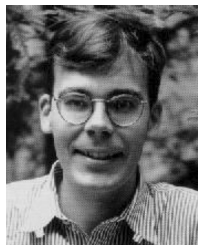

Axel Scherer received the B.S., M.S., and Ph.D. degrees from the New Mexico Institute of Mining and Technology, Socorro, in 1981, 1982, and 1985, respectively.

From 1985 to 1993, he was with the Quantum Device Fabrication Group, Bellcore. He is currently the Bernard E. Neches Professor of electrical engineering, applied physics, and physics at the California Institute of Technology, Pasadena, specializing in device microfabrication. His current research interests include design and fabrication of functional photonic, nanomagnetic, and microfluidic devices.